Joint geodynamic-geophysical inversion reveals passive subduction and accretion of the Ontong Java Plateau

Hao Dong[1], Liming Dai[1], Lijun Liu[2], Xiaodian Jiang[1], Sanzhong Li[1], Wei Gong[1], Liangliang wang[1], Di Wang[1], Zhong-Hai Li[3], and Shengyao Yu[1]

[1]Ocean University of China
[2]University of Illinois at Urbana Champaign
[3]University of Chinese Academy of Sciences

November 22, 2022

Abstract

In this study, we for the first time applied a joint geodynamic-geophysical inversion (JGGI) approach to oceanic plateau subduction models, and compared the subduction style and corresponding topography and Bouguer gravity of two representative subduction scenarios with passive or active collision. We showed that the case of passive collision of the Ontong Java Plateau (OJP) crust better explains the topography, gravity, and seismic data than the active collision scenario. This implies that the OJP did not control the regional dynamics during the collisional process. We conclude that previous studies may have overestimated the role of the OJP in triggering subduction initiation, subduction polarity reversal, and even Pacific Plate rotation.

Hosted file

`supplementary(combined).docx` available at https://authorea.com/users/523842/articles/598294-joint-geodynamic-geophysical-inversion-reveals-passive-subduction-and-accretion-of-the-ontong-java-plateau

Hosted file

`essoar.10512188.1.docx` available at https://authorea.com/users/523842/articles/598294-joint-geodynamic-geophysical-inversion-reveals-passive-subduction-and-accretion-of-the-ontong-java-plateau

Joint geodynamic-geophysical inversion reveals passive subduction and accretion of the Ontong Java Plateau

Hao Dong[1,2], Liming Dai[1,2]*, Lijun Liu[3]*, Xiaodian Jiang[1], Sanzhong Li[1,2]*, Wei Gong[1], Liangliang Wang[1,2], Di Wang[1,2], Zhong-Hai Li[4] & Shengyao Yu[1,2]

[1]Frontiers Science Center for Deep Ocean Multispheres and Earth System, Key Lab of Submarine Geosciences and Prospecting Techniques, MOE and College of Marine Geosciences, Ocean University of China, Qingdao 266100, China.

[2] Laboratory for Marine Geology, Qingdao National Laboratory for Marine Science and Technology, Qingdao 266237, China.

[3]University of Illinois at Urbana-Champaign, Urbana, IL, USA

[4] Key Laboratory of Computational Geodynamics, College of Earth and Planetary Sciences, University of Chinese Academy of Sciences, Beijing 100029, China

Corresponding author: Liming Dai (`dlming@ouc.edu.cn`), Lijun Liu (`ljliu@illinois.edu`) and Sanzhong Li (`sanzhong@ouc.edu.cn`)

Key Points:

- The joint geodynamic-geophysical inversion approach can help distinguish ambiguous dynamic behaviors of oceanic plateau subduction.

- The Bouguer gravity and other observations of Ontong Java Plateau favor the passive collision model over the active collision model.

- Ontong Java Plateau should have played a passive role in the collision process, implying the overestimation in previous studies.

Abstract

In this study, we for the first time applied a joint geodynamic-geophysical inversion (JGGI) approach to oceanic plateau subduction models, and compared the subduction style and corresponding topography and Bouguer gravity of two representative subduction scenarios with passive or active collision. We showed that the case of passive collision of the Ontong Java Plateau (OJP) crust better explains the topography, gravity, and seismic data than the active collision scenario. This implies that the OJP did not control the regional dynamics during the collisional process. We conclude that previous studies may have overestimated the role of the OJP in triggering subduction initiation, subduction polarity reversal, and even Pacific Plate rotation.

Plain Language Summary

The effect of the Ontong Java Plateau (OJP), the largest oceanic plateau on Earth, on subduction dynamics remains controversial. Proposed models for the evolution of the OJP range from dominantly "soft docking" that generates shallow subduction and little impact on nearby regions, to strong and active collision that results in deep plateau subduction, extensive accretion, subduction

1

polarity reversal, and even major plate reorganization. Determining the subduction depth and accretion volume of OJP is the key to resolving this dispute. In the former, the oceanic plateau undergoes shallow subduction with its upper and middle crusts slightly accreted into the island arc, leading to relatively low topography and a flat Bouguer gravity profile, consistent with observation. The latter case leads to deep subduction of the plateau lithosphere, resulting in high topography, low Bouguer gravity, and crustal structures that all violate observation.

1 Introduction

Oceanic plateau subduction is generally thought to play an important role in both the evolution of the downgoing plate(Hu et al., 2016; van Hunen et al., 2002; Mahlburg Kay & Mpodozis, 2002) and the tectonics of the overriding plate(Hu et al., 2021; L. Liu et al., 2010; Saleeby et al., 2003). However, most of these subduction events occurred during the geological past, with limited direct constraints on the nature and configuration of the putative plateaus(Z. Liu et al., 2021; Livaccari et al., 1981). Consequently, both the fate the subducting plate and the resulting tectonic implications remain to be further explored. In this study, we investigate the lithospheric deformation and physiographic architecture of the ongoing subducting Ontong Java Plateau (OJP) using a joint geodynamic-geophysical inversion (JGGI). Based on these results, we attempt to better understand the style of plateau subduction as well as the associated tectonic implications.

OJP is the largest extant oceanic plateau on Earth, co-formed with the Mesozoic-aged Manihiki Plateau (MP) and Hikurangi Plateau (HP)(Coffin & Eldholm, 1993; Taylor, 2006). By now, the MP has not reached the subduction zone, while the most of HP has been subducted into the mantle(Davy & Wood, 1994; Taylor, 2006). In comparison, the OJP encountered the southwest Pacific trench and collided with the Solomon Island Arc (SIA) during the Late Miocene (Fig. 1). This history of OJP subduction and collision is largely coincident with multiple nearby tectonic events, including subduction initiation, subduction polarity reversal, turning of the Tasman Sea seamount chain in the eastern Indo-Australian Plate (IAP), and rotation of the Pacific Plate, implying a potential causal relationship among them(Austermann et al., 2011; Knesel et al., 2008; Mann & Taira, 2004; Petterson et al., 1997; Phinney et al., 2004; Ramsay, 1985).

However, both the fate of OJP and its role in affecting these tectonic processes remain heavily debated. Many researchers claimed that the active subduction of the OJP-bearing Pacific Plate dominantly shaped the tectonics of the subduction zone and even triggered the rotation of the Pacific Plate(Almeida, Riel, Rosas, Duarte, & Kaus, 2022; Almeida, Riel, Rosas, Duarte, & Schellart, 2022; Knesel et al., 2008; Ramsay, 1985; Sun et al., 2021; Tao et al., 2020). The presumed histories of OJP evolution among these models fall into two end-member scenarios: some proposed that most of the plateau crust has been subducted to >200 km deep by now(Almeida, Riel, Rosas, Duarte, & Kaus, 2022; Almeida, Riel, Rosas, Duarte, & Schellart, 2022), while others suggested the crust was

mostly or entirely accreted to the overriding island arc(Sun et al., 2021; Tao et al., 2020). In contrast to the above active role of OJP, some studies believed that OJP collision was a passive "soft docking" event, which led to little impact on subduction initiation and other tectonic events(Petterson et al., 1997; L. Wang et al., 2022).

These inconsistencies on the perceived OJP evolution should reflect the lack of knowledge on the subduction style of OJP. To resolve this key uncertainty, we designed a JGGI approach. We first utilize forward geodynamic modeling to reproduce different evolutionary histories of the subduction process as previously proposed. Then we examine their associated gravity and topography to constrain the resulting present-day density structure of the crust and mantle lithosphere around the subduction zone, with a focus on the oceanic plateau. In addition, we also incorporate available seismic images to further evaluate the structural configuration of the OJP features, especially at shallow depths where the seismic resolving power is high (Fig. 1d). This JGGI approach has been proved to be able to constrain the shallow crustal features, such as salt structures(Baumann et al., 2014). Our attempt represents the first application of this approach to subduction zones.
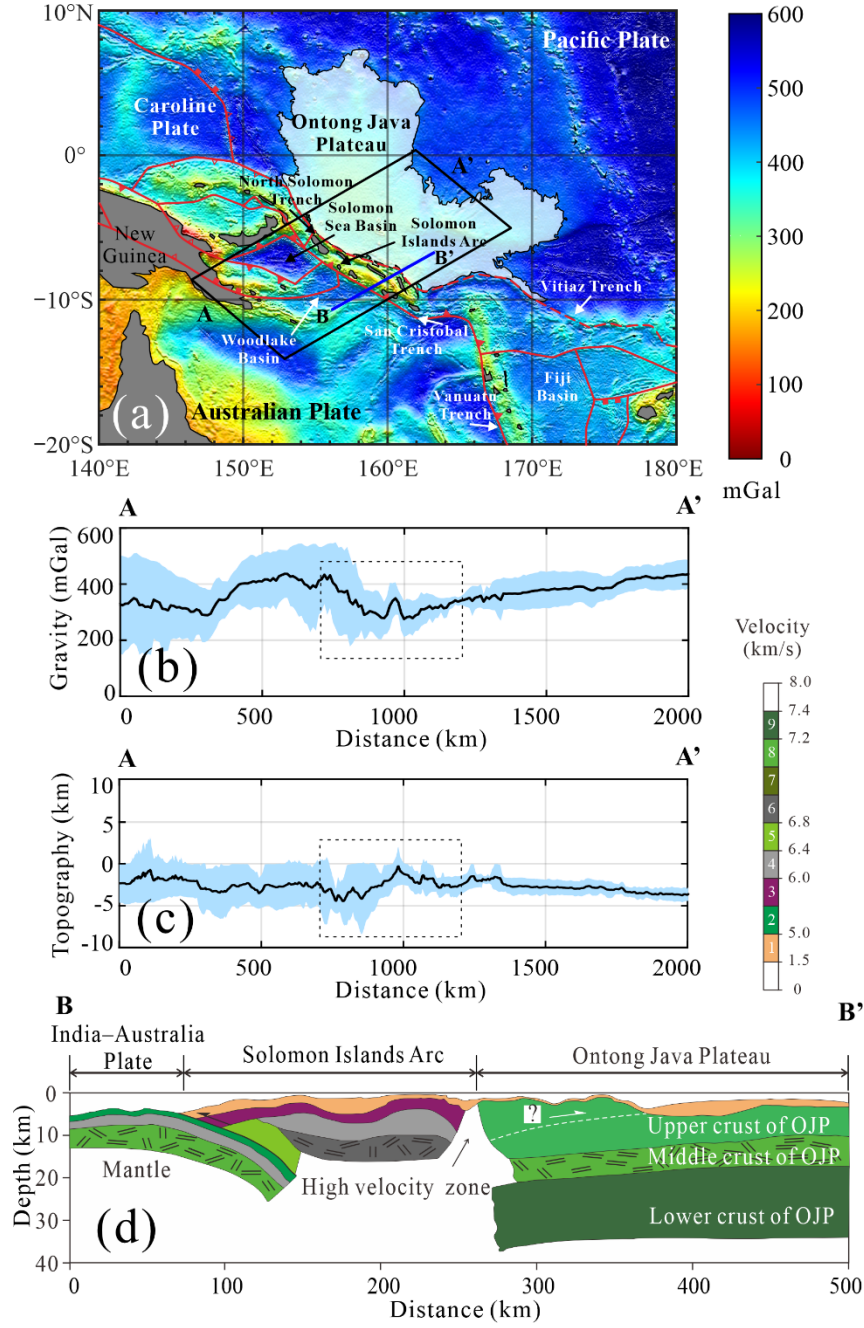
Fig. 1. (a) The Bouguer gravity anomaly (WGM2012) with plate boundaries(Austermann et al., 2011; Balmino et al., 2012). The white shade represents OJP and the black shadow represents land. The black rectangle outlines

the location of gravity profiles in Fig. 1b. (b) Bouguer gravity anomaly profiles across the Ontong Java Plateau(Balmino et al., 2012). (c) Topography profiles across the Ontong Java Plateau(Amante & Eakins, 2009). These profiles have been aligned by cross-correlation. The blue area represents the range of data in the box shown in (a), and the black line represents the median of the data. The dotted box indicates the location of the OJP and the SIA. (d) The crustal structure of Ontong Java Plateau and Solomon Islands Arc based on the seismic profile(Mann & Taira, 2004; Miura et al., 2004).

2 Methods

The numerical model of this study is based on finite difference method (FDM) and marker-in-cell (MIC) technology with a staggered grid. The implemented code I2VIS is open source(Gerya & Yuen, 2003; Perchuk et al., 2020) and widely used in simulating subduction zone dynamics(Dai et al., 2018; Huangfu et al., 2018; Li et al., 2015). We also consider the prograde metamorphism within the subducting plate. The data we adopted come from a previous study on this phase transformation (Y. Wang et al., 2019).

In the Bouguer gravity calculation, models are regarded as two-dimensional bodies and numerical integration is carried out. See supplementary materials for the details of method and initial model. In order to directly compare the measured gravity data and the model results, we first convert the spherical coordinates of the measured gravity into Cartesian coordinates, and then align them relative to the reference normal seafloor.

3 Results

Here, we considered two contrasting geodynamic scenarios: 1) OJP passively collides with SIA at a relatively small speed; 2) OJP actively collides with SIA at a faster speed. The JGGI approach allows us to evaluate the outcome of subduction and accretion of oceanic plateau during these collision models. To best reproduce the key subduction features revealed by the seismic image (Fig, 1d), as well as the main gravity features, we adjusted and tested a series of model parameters, including the width of the island arc, the density of the upper crust of the island arc, the depth and inclination of the Moho, the lithospheric thickness of the new oceanic basin, and the initial position of the plateau. Tests of model parameters and the iterative search for the optimal settings are in the supplementary file (Table S3). Among these processes, a quantitative calculation of the gravity contribution of various tectonic features from the geodynamic model allows further evaluation of their causes and consequences. Eventually, we locate the preferred OJP model that is consistent with measured Bouguer gravity anomaly, surface topography, and seismic imaging.

3.1 Passive collision model

At the initial stage of collision, the plateau partially enters the subduction zone (Fig. 2a). There is no obvious deformation in the plateau, implying overall "soft docking", consistent with previous studies(Petterson et al., 1997; L. Wang et al.,

5

2022). In the subduction zone, the low-density crust of the plateau contributes a negative gravity anomaly, resulting in an obvious trough on the gravity curve. Continuous fast motion of the overriding plate results in downward bending and partial subduction of the plateau, causing its gravity effect to decrease (Fig. 2b). The upper and middle plateau crust accretes to the island arc, while the rest enters the subduction zone. Correspondingly, the gravity trough disappears not only due to the filling of trench during accretion but also to the progressive metamorphism of plateau crust (Fig. S3). The lithosphere of the island arc suffers horizontal compression, resulting in two synclines and one anticline. Therefore, the gravity anomaly presents a wide and gentle W-shaped profile.

As collision continues, the accretion body becomes larger and its gravity amplitude increases (Fig. 2c). The gravity trough of ~200 mGal at the trench evolves into a relatively flat pattern with even a locally elevated signal. The island arc further deforms and shortens, and its corresponding gravity profile shrinks into a tighter fold-structure. At this time, subduction with an opposite polarity initiates at the left side of the arc. This process does not generate a district gravity signal, because strong deformation on the left side of the island arc dominates the total gravity response.

In the final stage, the new subduction is fully developed while the plateau has stopped subduction and begins to separate from the subducted slab (Fig. 2d). The slab break-off below the plateau is a result of its buoyancy contrast with that of the plateau(Hu & Liu, 2016). Another factor is partial melting above the subducted slab that locally decreases the rheological strength of the slab(Coleman & Kroenke, 1981; Hanyu et al., 2017; Ramsay, 1985). During this process, the accretion of plateau crust largely comes to an end. In this model, the total amount of accreted plateau crust is minor. At the end of the accretion process, the new subduction zone releases upper-plate compression, causing the crust of the island arc to gradually relax and extend, which results in a decline of topography and a decrease of gravity anomaly above the arc.

In this passive collision case, the modeled Bouguer gravity anomaly finally evolves into a relatively flat pattern, with a positive gravity anomaly value of ~250 mGal (Fig. 2). On one hand, this results from shallow subduction of the plateau. In practice, active obduction of the overriding plate leads to shallow subduction of the plateau front (Fig. 2a, b), which is significantly weakened after subduction with an opposite polarity (Fig. 2c, d). The failed plateau subduction only generates a minor amount of mass loss, as corresponds to an elevated gravity anomaly. On the other hand, the disappearance of the gravity trough along the trench indicates that the gravity fluctuation attenuates toward the present. This reflects that 1) the accumulation of plateau crust at the trench raises the topography close to sea surface and the value of gravity anomaly; 2) the subducted oceanic plateau undergoes progressive metamorphism to increase its density (Fig. S3); 3) the mantle uplift at the SIA edge leads to the thinning of the crust and the elevation of the Moho surface. The flat gravity profile also

indicates that formation of the new subduction zone helps to release upper-plate compression. Correspondingly, the horizontal compression of the SIA crust is significantly weakened and even switches to extension in the shallow part, a process that relaxes the island arc anticline causing subsiding seafloor and shallowing Moho (Fig. 2c, d).
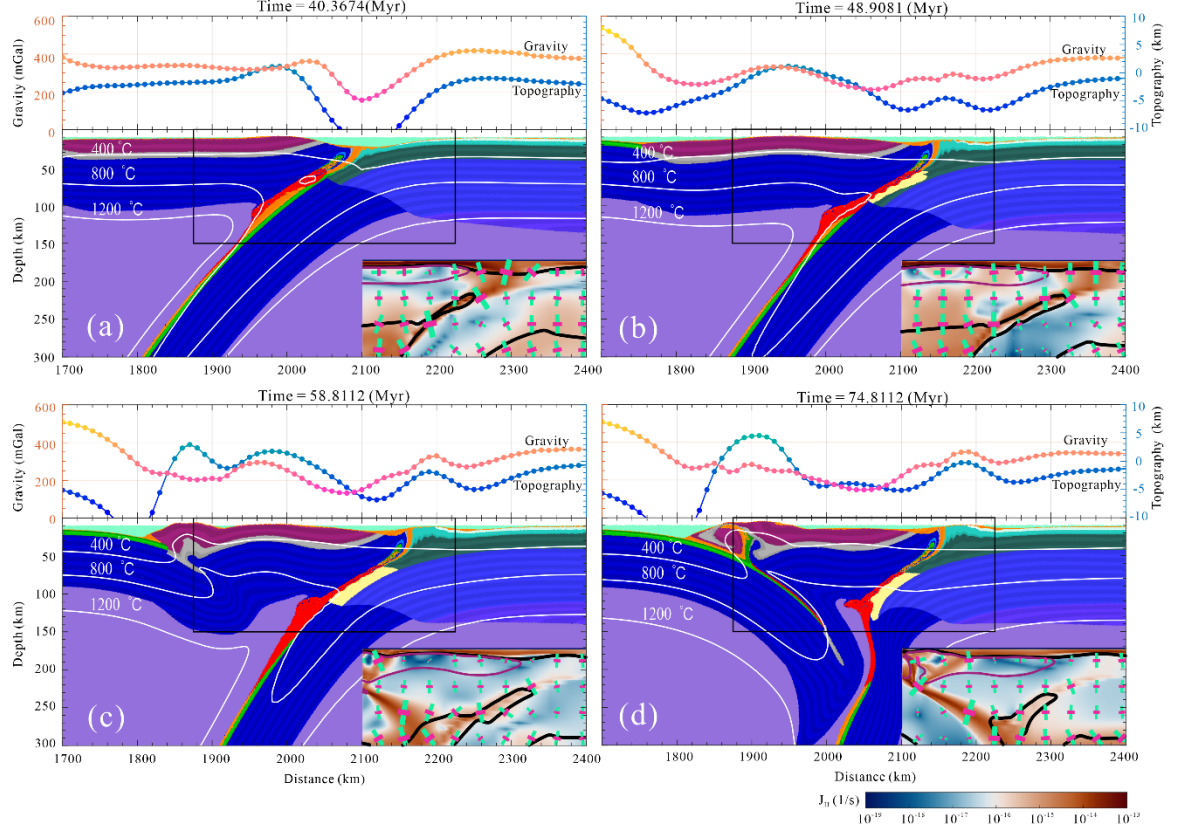

Fig. 2. The passive collision model. (a-d) Model structures (lower) with the associated profiles of Bouguer gravity and topography (upper). White solid lines are temperature contours. The forward geodynamic model results include the evolving compositional features and the second invariant of the deviatoric strain rate (J_{II}), which is shown in the lower right corner of each panel. Black lines outline the lithosphere. Purple lines outline the SIA crust. The crosses indicate the direction of strain rate (green bars represent extension and red bars represent compression).

3.2 Active collision model

Similar to the early stage of the passive collision model, the active collision model also witnesses a clear gravity trough above the plateau front (Fig. 3a). Meanwhile, the continuous convergence leads to a new subduction zone to nu-

cleate to the left of the island arc. As the collision continues, fast subduction of the plate from the right causes continuous OJP crust accretion onto the island arc (Fig. 3b). This is because deformation of the plateau is stronger than that in the passive collision model, as also implied by the more prominent second invariant of strain rate. As a result of the fast convergence, the island arc crust is rapidly thickened by compression, whose gravity effect dominates that of the incipient subduction zone underneath. The larger extent of accretion locally thickens the OJP crust and raises its topography closer to sea level.

Accretion of buoyant OJP crust allows the underlying dense plateau lithosphere to continue subduction, a process that generates more dynamic subsidence than in the passive collision case, pulling the surface further down. Consequently, the subsiding seafloor of the region with the deepened Moho of the island arc reduce the regional Bouguer gravity (Fig. 3c). Continuous collision and accretion force the crust of the island arc to grow thicker, with its surface eventually above sea level and Moho at a greater depth (Fig. 3d). In this case, due to the removal of the buoyant plateau crust from the downgoing plateau lithosphere, slab break-off does not occur.

Both the isostatically deeper Moho and greater dynamic subsidence in the passive case help to reduce the gravity anomaly. Consequently, the present-day Bouguer gravity anomaly is much lower with multiple troughs whose minimum values approach 0 mGal (Fig. 3d). This is closely related to the strong dynamic effect of the plateau. On the one hand, the plateau actively collides with the island arc without slab break-off, resulting in a subduction depth of the plateau that exceeds 200 km, with prominent OJP crustal mass loss into the mantle (Fig. 3d). On the other hand, the compression of the island arc is stronger and more persistent (Fig. 3b, c) than that in the passive model, causing the topography to increase and the gravity to decrease. As a result of the fast convergence, the island arc crust is rapidly thickened by compression with its final surface above sea level and the Moho further deepened, whose gravity effect dominates that of the incipient subduction zone underneath. Collectively, the gravity in the active collision case is much lower than that of the passive collision case.
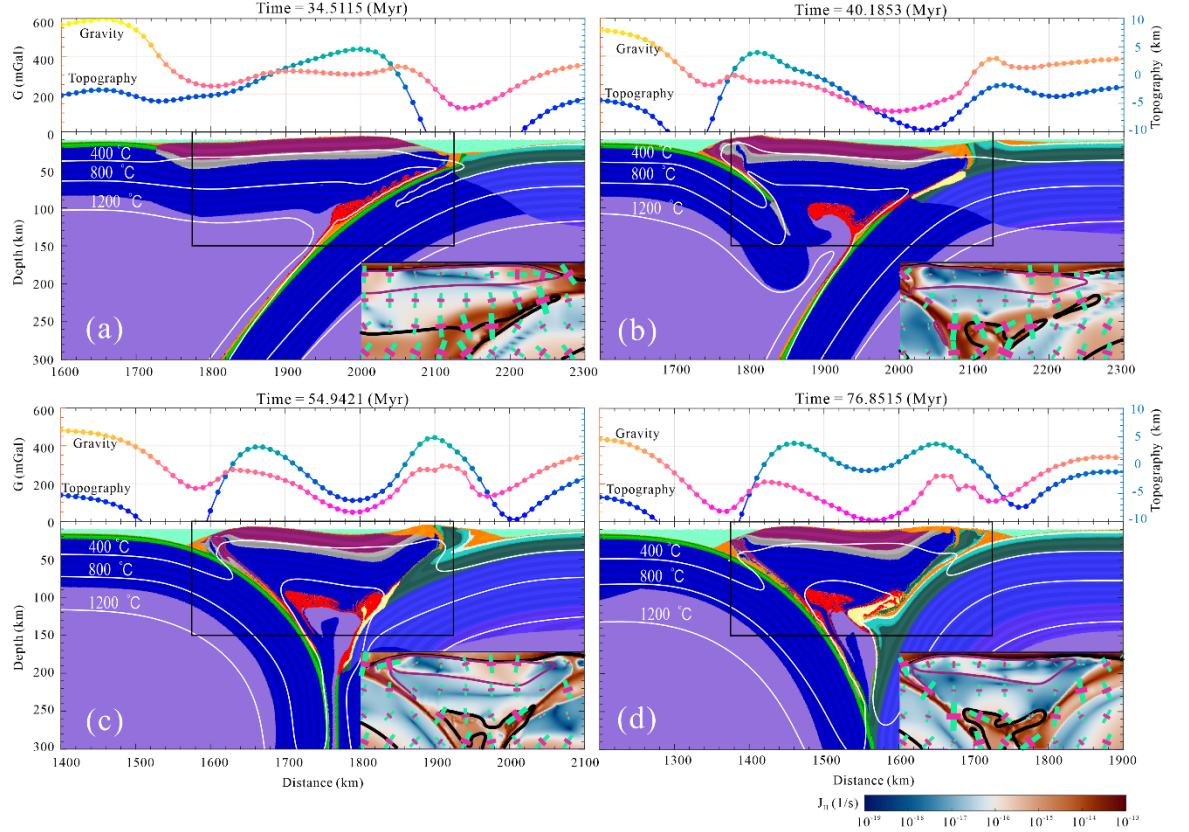
Fig. 3. The active collision model. (a-d) Model structures (lower) with the associated profiles of Bouguer gravity and topography (upper). The forward geodynamic model results include the evolving compositional features and the second invariant of the deviatoric strain rate (J_{II}), which is shown in the lower right corner of each panel.

4 Discussion and Conclusion

4.1 The JGGI constraints on OJP subduction

By tracking the model evolution and associated gravity anomaly, we found that there is an intuitive correlation between the deforming lithospheric features and gravity (Figs. 2, 3). This means the observed present-day gravity profile across the study area (Fig. 1) provides a promising constraint on the style of OJP subduction and collision. The second constraint is topography, which serves as a supplementary of shallow information (Fig. 4a). The third important constraint comes from seismic imaging, which provides important structural information on the resulting lithospheric configuration (Fig. 1d). This includes ~100 km wide OJP crust accreted to the SIA(Miura et al., 2004; Petterson et al., 1997), as corresponds to a locally elevated gravity anomaly with a peak value of ~400 mGal (Balmino et al., 2012). Another unique seismic feature is a high-velocity

9

anomaly (Fig. 1d) between OJP and SIA(Mann & Taira, 2004; Miura et al., 2004), which is also associated with a minor peak in gravity (Balmino et al., 2012). Finally, the central part of SIA develops into a syncline (Fig. 1d), and the corresponding gravity anomaly shows a trough as low as 200 mGal (Balmino et al., 2012).

The above gravity and seismic observations match the results from the passive collision model (Fig. 4b, c, d) significantly better than those of the active collision model (Fig. 4b, e, f). In general, the observed Bouguer gravity reflects the combined effect of crust and mantle lithosphere. In the passive collision case, both the relatively thin SIA crust and the limited dynamic subsidence due to failed subduction of the OJP lithosphere generate regionally high gravity with a flat profile, consistent with observation (Fig. 4b). In the active collision case, continuous subduction of the oceanic plateau leads to stronger compression and thicker SIA crust, which, together with prominent dynamic subsidence, result in much a reduced magnitude of Bouguer gravity (Fig. 4b, e). This difference is clearly reflected in the island arc. For example, the minimum value of gravity anomaly in the passive collision case is about 149.9 mGal, only slightly lower than the observation (Fig. 4b). In contrast, the minimum gravity in the active collision case is close to zero, much smaller than the observation (Fig. 4b). This is because in the active model (Fig. 4f, h) subduction of the oceanic plateau contributes more anomalies (-113.0 mGal) to nearby regions, and the more shortened island arc has a deeper Moho, and thus a greater negative gravity contribution (-615.2 mGal) than in the passive situation.

The above conclusion is further supported by other observational constraints. First, the topography generated by the passive collision case is more consistent observation than that in the active collision case (Fig. 4a). Stress relaxation in the passive collision case after subduction initiation leads to low topography in the middle SIA, which is more balanced. Second, the gravity contribution of the upper crust of the accretion body in the passive collision case is greater than that in the active collision case. The causes of the local gravity variation include not only crustal deformation, but also the resulting prograde metamorphism (Fig. S3). Therefore, the upper crust generates positive anomalies, resulting in local peaks (Fig. 4d). Third, according to our previous research, the passive collision models with shallow subduction are also more consistent with other observations of nearby regions, such as tomography and the Benioff zone(L. Wang et al., 2022). Consequently, such passive collision models may better reflect the actual histories of OJP evolution.
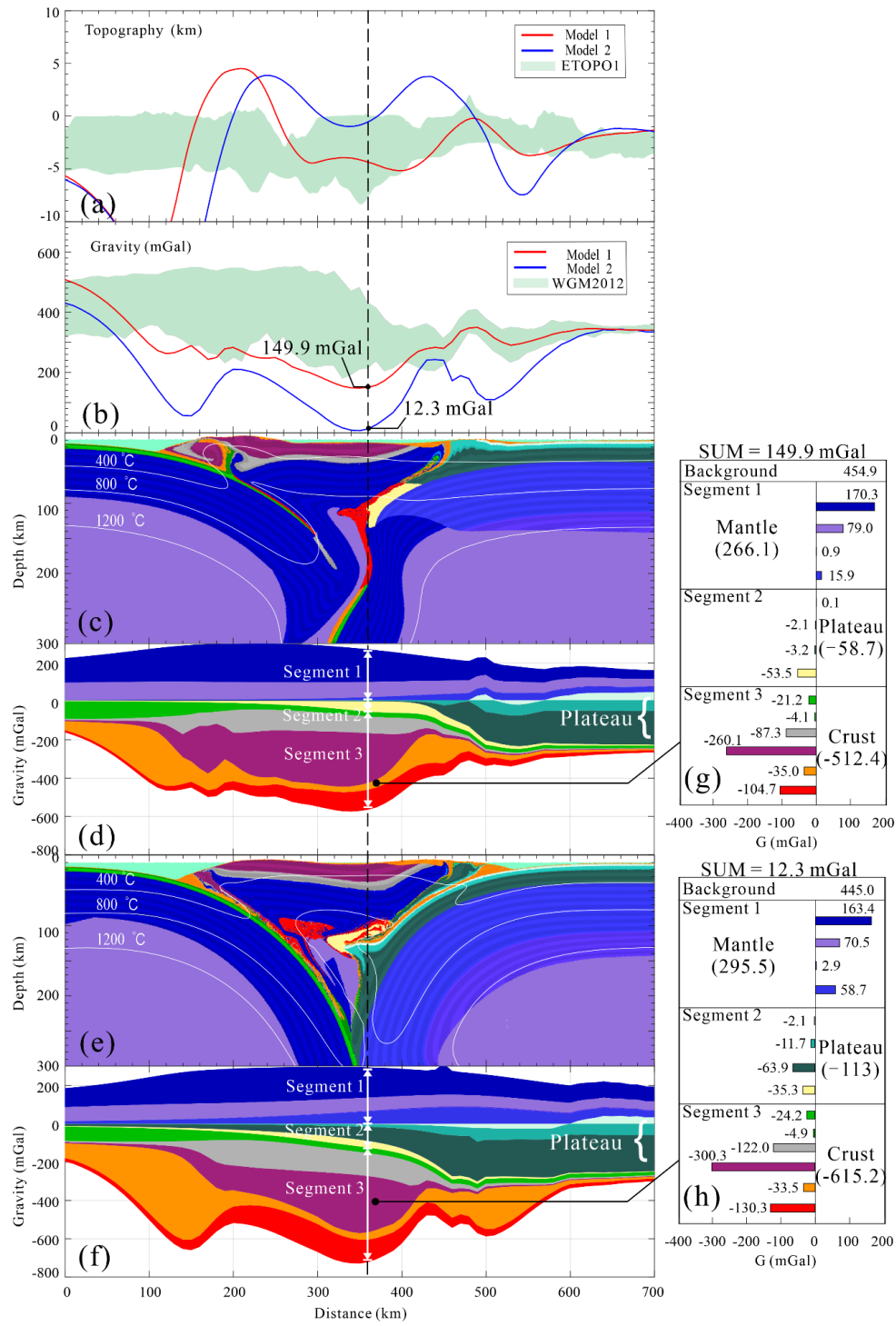
Fig. 4. (a-b) Modeled surface topography and the Bouguer gravity anomalies. Model 1: passive collision model; Model 2: active collision model; ETOPO1: the observation of OJP(Amante & Eakins, 2009); WGM2012: the observation of OJP(Baumann et al., 2014). The numbers (149 & 12.3 mGal) represent the gravity anomaly at x = 360 km. (c) The final result of the passive collision model. (d) Gravity composition area chart of each composition of the passive collision model. Different colors represent the gravity anomaly contribution from different compositions. These colors are similar to the colors used in Fig. 4c. (e) The final result of the active collision model. (f) Gravity composition area chart of each composition of the active collision model. (g) Histogram of gravity composition of the passive collision model at x = 360 km, including three segments (1: Mantle; 2: Oceanic plateau; 3: Crust). (h) Histogram of gravity composition of the active collision model at x = 360 km.

4.2 OJP experienced neither deep subduction nor strong accretion

Some previous studies argued that OJP may have subducted to greater than 200 km(Mann & Taira, 2004; Phinney et al., 2004). Some numerical models also showed that the oceanic plateau could subduct deep, even in a gravity-driven model(Almeida, Riel, Rosas, Duarte, & Kaus, 2022; Almeida, Riel, Rosas, Duarte, & Schellart, 2022). Here we show that this scenario will result in the thickened SIA crust, deep subduction of the plateau crust and negative dynamic topography, all of which lead to more prominent negative gravity anomaly and stronger topographic gradients than those observed (Fig. 4a). In contrast, the scenario with OJP shallowly subducted better matches these observations. Effectively, this analysis suggests that the shallow subduction models are better in describing the collisional process between the OJP and the SIA than the deep subduction models. Although not applicable to the OJP subduction, active collision models are suitable for describing deep subduction of other plateaus, such as the Hikurangi Plateau (Fig. S4) and the Nazca Ridge, which have been confirmed to have experienced deep subduction(Davy & Wood, 1994; Hu et al., 2016; Z. Liu et al., 2021; Reyners et al., 2011; Taylor, 2006).

Some previous studies claimed that the accretion of the plateau crust can result in subduction initiation(Almeida, Riel, Rosas, Duarte, & Kaus, 2022; Almeida, Riel, Rosas, Duarte, & Schellart, 2022; Sun et al., 2021; Tao et al., 2020; L. Wang et al., 2022). In these models, the plateau either strongly accreted to the island arc or completely decoupled from the subducted mantle during the collision. However, the actual accreted width (~ 100km) shown in the seismic profile (Fig. 1d) is significantly less than that among the above models(Mann & Taira, 2004; Miura et al., 2004). According to our results (Fig. 3), the accretion body corresponds to a clear peak in the gravity anomaly profile, and its magnitude increases with increasing accretion volume. Excessive accretion makes this gravity feature significantly higher than that of nearby regions, inconsistent with observation (Fig. 1d). In addition, as shown in the results, strong accretion also controls the shape of the island arc and affects the development of the anticline (Fig. 3b-d). The scale of the simulated accretion body during

the strong accretion scenario is also inconsistent with reality, where the OJP experienced moderate accretion with accreted material only at a local scale (Fig. 1d). This implies that the OJP crust does not entirely detach from the mantle as described in some previous models(Sun et al., 2021; Tao et al., 2020). Therefore, the active collision model with strong accretion may not reflect the actual situation of the OJP subduction.

4.3 OJP played a passive role in the collision process

Through the JGGI approach, we quantitatively analyze and reinterpret multiple observations associated with OJP, and conclude that this plateau did not experience deep subduction or strong collision. Instead, it is likely forced to undergo intermittent subduction with moderate accretion(Coleman & Kroenke, 1981). The lithospheric deformation of OJP mainly occurred after the subduction initiation of the Solomon trench. This implies that the OJP played a minor role in the subduction initiation(L. Wang et al., 2022). Although previous studies have argued that active collision between the oceanic plateau and the island arc can trigger subduction initiation(Almeida, Riel, Rosas, Duarte, & Kaus, 2022; Almeida, Riel, Rosas, Duarte, & Schellart, 2022; Sun et al., 2021; Tao et al., 2020; L. Wang et al., 2022), our results demonstrate that this should not apply to the OJP. Similarly, we suggest that an oceanic plateau under passive collision like OJP is difficult to cause the rotation of the Pacific Plate as claimed previously(Austermann et al., 2011; Knesel et al., 2008; Petterson et al., 1997; Phinney et al., 2004; Ramsay, 1985). Both geological records and model results show that the SIA and OJP have experienced limited deformation, which indicates that the interaction between OJP and the upper plate has been weak since 25 - 20 Ma, consistent with the OJP playing a minor braking role of the Pacific motion(Petterson et al., 1997; L. Wang et al., 2022). Consequently, the rotation of the Pacific Plate begs for another mechanism. According to our model, an initial deceleration triggers the slab break-off, where the resulting loss of slab pull would slow down the plate motion, as is a possible explanation for the Pacific rotation.

On the other hand, our numerical models suffer from the uncertain initial condition and computational accuracy, so they cannot perfectly reproduce the gravity anomaly of the entire study region. One such mismatch is the IAP-SIA region (Figs. 1a, 4a) where the initial condition does not attempt to capture the corresponding lithospheric structure. Nevertheless, the observed gravity anomaly and topography further east in the subduction zone display smaller variations that are properly reproduced in our modeling result (Fig. 4a).

Open Research

Data Availability Statement

The Bouguer gravity anomaly model WGM2012 is available at http://bgi.obs-mip.fr/data-products/grids-and-models/wgm2012-global-model/. The global crustal model Crust 1.0 is available at https://igppweb.ucsd.edu/~gabi/crust1.html. The global relief model is available at https://ngdc.noaa.gov/mgg/global/global.html. All related modeling data will be provided in Zenodo (https://zenodo.org/record/6984086).

References

Almeida, J., Riel, N., Rosas, F. M., Duarte, J. C., & Schellart, W. P. (2022). Polarity-reversal subduction zone initiation triggered by buoyant plateau obstruction. *Earth and Planetary Science Letters*, *577*, 117195. https://doi.org/https://doi.org/10.1016/j.epsl.2021.117195

Almeida, J., Riel, N., Rosas, F. M., Duarte, J. C., & Kaus, B. (2022). Self-replicating subduction zone initiation by polarity reversal. *Communications Earth & Environment*, *3*(1). https://doi.org/10.1038/s43247-022-00380-2

Amante, C., & Eakins, B. W. (2009). ETOPO1 1 Arc-Minute Global Relief Model: Procedures, Data Sources and Analysis. *NOAA Technical Memorandum NESDIS NGDC-24*, (March). https://doi.org/10.1594/PANGAEA.769615

Austermann, J., Ben-Avraham, Z., Bird, P., Heidbach, O., Schubert, G., & Stock, J. M. (2011). Quantifying the forces needed for the rapid change of Pacific plate motion at 6Ma. *Earth and Planetary Science Letters*, *307*(3), 289–297. https://doi.org/https://doi.org/10.1016/j.epsl.2011.04.043

Balmino, G., Vales, N., Bonvalot, S., & Briais, A. (2012). Spherical harmonic modelling to ultra-high degree of Bouguer and isostatic anomalies. *Journal of Geodesy*, *86*(7), 499–520. https://doi.org/10.1007/s00190-011-0533-4

Baumann, T. S., Kaus, B. J. P., & Popov, A. A. (2014). Constraining effective rheology through parallel joint geodynamic inversion. *Tectonophysics*, *631*, 197–211. https://doi.org/10.1016/j.tecto.2014.04.037

Coffin, M. F., & Eldholm, O. (1993). Scratching the surface: Estimating dimensions of large igneous provinces. *Geology*, *21*(6), 515–518. https://doi.org/10.1130/0091-7613(1993)021<0515:STSEDO>2.3.CO;2

Coleman, P. J., & Kroenke, L. W. (1981). Subduction without volcanism in the Solomon Islands arc. *Geo-Marine Letters*, *1*(2), 129–134. https://doi.org/10.1007/BF02463330

Dai, L., Li, S., Li, Z. H., Somerville, I., Suo, Y., Liu, X., et al. (2018). Dynamics of exhumation and deformation of HP-UHP orogens in dou-

ble subduction-collision systems: Numerical modeling and implications for the Western Dabie Orogen. *Earth-Science Reviews*, *182*(238), 68–84. https://doi.org/10.1016/j.earscirev.2018.05.005

Davy, B., & Wood, R. (1994). Gravity and magnetic modelling of the Hikurangi Plateau. *Marine Geology*, *118*(1–2), 139–151. https://doi.org/10.1016/0025-3227(94)90117-1

Gerya, T. v., & Yuen, D. A. (2003). Characteristics-based marker-in-cell method with conservative finite-differences schemes for modeling geological flows with strongly variable transport properties. *Physics of the Earth and Planetary Interiors*, *140*(4), 293–318. https://doi.org/10.1016/j.pepi.2003.09.006

Hanyu, T., Tejada, M. L. G., Shimizu, K., Ishizuka, O., Fujii, T., Kimura, J.-I., et al. (2017). Collision-induced post-plateau volcanism: Evidence from a seamount on Ontong Java Plateau. *Lithos*, *294–295*, 87–96. https://doi.org/https://doi.org/10.1016/j.lithos.2017.09.029

Huangfu, P., Li, Z. H., Gerya, T., Fan, W., Zhang, K. J., Zhang, H., & Shi, Y. (2018). Multi-terrane structure controls the contrasting lithospheric evolution beneath the western and central–eastern Tibetan plateau. *Nature Communications*, *9*(1), 1–11. https://doi.org/10.1038/s41467-018-06233-x

Hu, J., & Liu, L. (2016). Abnormal seismological and magmatic processes controlled by the tearing South American flat slabs. *Earth and Planetary Science Letters*, *450*. https://doi.org/10.1016/j.epsl.2016.06.019

Hu, J., Liu, L., Hermosillo, A., & Zhou, Q. (2016). Simulation of late Cenozoic South American flat-slab subduction using geodynamic models with data assimilation. *Earth and Planetary Science Letters*, *438*, 1–13. https://doi.org/10.1016/j.epsl.2016.01.011

Hu, J., Liu, L., & Gurnis, M. (2021). Southward expanding plate coupling due to variation in sediment subduction as a cause of Andean growth. *Nature Communications*, *12*(1). https://doi.org/10.1038/s41467-021-27518-8

van Hunen, J., van den Berg, A. P., & Vlaar, N. J. (2002). On the role of subducting oceanic plateaus in the development of shallow flat subduction. *Tectonophysics*, *352*(3–4), 317–333. https://doi.org/10.1016/S0040-1951(02)00263-9

Knesel, K. M., Cohen, B. E., Vasconcelos, P. M., & Thiede, D. S. (2008). Rapid change in drift of the Australian plate records collision with Ontong Java plateau. *Nature*, *454*(7205), 754–757. https://doi.org/10.1038/nature07138

Liu, L., Gurnis, M., Seton, M., Saleeby, J., Müller, R. D., & Jackson, J. M. (2010). The role of oceanic plateau subduction in the Laramide orogeny. *Nature Geoscience*, *3*(5). https://doi.org/10.1038/ngeo829

Liu, Z., Dai, L., Li, S., Wang, L., Xing, H., Liu, Y., et al. (2021). When plateau meets subduction zone: A review of numerical models. *Earth-Science Reviews*, *215*(238), 103556. https://doi.org/10.1016/j.earscirev.2021.103556

Livaccari, R. F., Burke, K., & Şengör, A. M. C. (1981). Was the Laramide orogeny related to subduction of an oceanic plateau? *Nature*, *289*(5795). https://doi.org/10.1038/289276a0

Li, Z. H., Liu, M. Q., & Gerya, T. (2015). Material transportation and fluid-melt activity in the subduction channel: Numerical modeling. *Science China Earth Sciences*, *58*(8), 1251–1268. https://doi.org/10.1007/s11430-015-5123-5

Mahlburg Kay, S., & Mpodozis, C. (2002). Magmatism as a probe to the Neogene shallowing of the Nazca plate beneath the modern Chilean flat-slab. *Journal of South American Earth Sciences*, *15*(1), 39–57. https://doi.org/10.1016/S0895-9811(02)00005-6

Mann, P., & Taira, A. (2004). Global tectonic significance of the Solomon Islands and Ontong Java Plateau convergent zone. *Tectonophysics*, *389*(3-4 SPEC.ISS.), 137–190. https://doi.org/10.1016/j.tecto.2003.10.024

Miura, S., Suyehiro, K., Shinohara, M., Takahashi, N., Araki, E., & Taira, A. (2004). Seismological structure and implications of collision between the Ontong Java Plateau and Solomon Island Arc from ocean bottom seismometer–airgun data. *Tectonophysics*, *389*(3), 191–220. https://doi.org/https://doi.org/10.1016/j.tecto.2003.09.029

Perchuk, A. L., Gerya, T. v, Zakharov, V. S., & Griffin, W. L. (2020). Building cratonic keels in Precambrian plate tectonics. *Nature*, *586*(7829), 395–401. https://doi.org/10.1038/s41586-020-2806-7

Petterson, M. G., Neal, C. R., Mahoney, J. J., Kroenke, L. W., Saunders, A. D., Babbs, T. L., et al. (1997). Structure and deformation of north and central Malaita, Solomon Islands: tectonic implications for the Ontong Java Plateau-Solomon arc collision, and for the fate of oceanic plateaus. *Tectonophysics*, *283*(1), 1–33. https://doi.org/https://doi.org/10.1016/S0040-1951(97)00206-0

Phinney, E. J., Mann, P., Coffin, M. F., & Shipley, T. H. (2004). Sequence stratigraphy, structural style, and age of deformation of the Malaita accretionary prism (Solomon arc–Ontong Java Plateau convergent zone). *Tectonophysics*, *389*(3), 221–246. https://doi.org/https://doi.org/10.1016/j.tecto.2003.10.025

Ramsay, W. R. H. (1985). Polarity reversal in the Solomon Islands arc. *Nature*, *318*(6044), 391–392. https://doi.org/10.1038/318391b0

Reyners, M., Eberhart-Phillips, D., & Bannister, S. (2011). Tracking repeated subduction of the Hikurangi Plateau beneath New Zealand. *Earth and Planetary Science Letters*, *311*(1–2), 165–171. https://doi.org/10.1016/j.epsl.2011.09.011

Saleeby, J., Ducea, M., & Clemens-Knott, D. (2003). Production and loss of high-density batholithic root, southern Sierra Nevada, California. *Tectonics*, *22*(6). https://doi.org/10.1029/2002tc001374

Sun, B., Kaus, B. J. P., Yang, J., Lu, G., Wang, X., Wang, K., & Zhao, L. (2021). Subduction Polarity Reversal Triggered by Oceanic Plateau Accretion: Implica-

tions for Induced Subduction Initiation. *Geophysical Research Letters*, *48*(24), e2021GL095299. https://doi.org/https://doi.org/10.1029/2021GL095299

Tao, J., Dai, L., Lou, D., Li, Z.-H., Zhou, S., Liu, Z., et al. (2020). Accretion of oceanic plateaus at continental margins: Numerical modeling. *Gondwana Research*, *81*, 390–402. https://doi.org/https://doi.org/10.1016/j.gr.2019.11.015

Taylor, B. (2006). The single largest oceanic plateau: Ontong Java–Manihiki–Hikurangi. *Earth and Planetary Science Letters*, *241*(3–4), 372–380. https://doi.org/10.1016/J.EPSL.2005.11.049

Wang, L., Dai, L., Gong, W., Li, S., Jiang, X., Foulger, G. R., et al. (2022). Subduction initiation at the Soloman back-arc basin: Contributions from both island arc rheological strength and oceanic plateau collision. *Earth and Space Science Open Archive*, 19. https://doi.org/10.1002/essoar.10510166.1

Wang, Y., Zhang, L., Li, Z.-H., Li, Q., & Bader, T. (2019). The Exhumation of Subducted Oceanic-Derived Eclogites: Insights From Phase Equilibrium and Thermomechanical Modeling. *Tectonics*, *38*. https://doi.org/10.1029/2018TC005349

Table S2 Parameters of the materials in the numerical mode

Material	状态	ρ_0 (kgm^{-3})	Cp (Jkg^{-1}K^{-1})	K[b] (Wm^{-1}K^{-1})	$T_{solidus}$[c] (k)	$T_{liquidus}$[c] (k)	Hr (μWm^{-3})
Air	−	1	100	20	−	−	0
Water	−	1000	3330	20	−	−	0
Sediment	Soild	2700	1000	K1	TS1	TL1	2
	Liquid	2500					
Upper continental crust	Soild	2900	1000	K1	TS1	TL1	2
	Liquid	2500					
Lower continental crust	Soild	3000	1000	K2	TS2	TL2	0.5
	Liquid	2500					
Oceanic crust	Soild	3000	1000	K2	TS2	TL2	0.25
	Liquid	2900					
Mantle	Soild	3300	1000	K3	−	−	0.022
	Liquid	2700					
Weak mantle	Soild	3300	1000	K3	−	−	0.022
	Liquid	2700					
Upper oceanic plateau crust	Soild	2730	1000	K2	TS2	TL2	0.25
	Liquid	2900					
Middle oceanic plateau crust	Soild	2850	1000	K2	TS2	TL2	0.25
	Liquid	2900					
Lower oceanic plateau crust	Soild	3030	1000	K2	TS2	TL2	0.25
	Liquid	2900					
Oceanic plateau mantle 1	Soild	3290	1000	K3	−	−	0.022
	Liquid	2700					
Oceanic plateau mantle 2	Soild	3290	1000	K3	−	−	0.022
	Liquid	2700					

a. $\rho0$ = reference density; Cp = specific heat capacity; K = thermal conductivity; $T_{solidus}$ = Solidus temperature; $T_{liquidus}$ = iquidus temperature; Hr=rad compressibility; sin (φ_{ff}) = effective friction coefficient.

b. K1=[0.64+807/(TK+77)]exp(0.00004P); K2=[1.18+474/(TK+77)]exp(0.00004P); K3=[0.73+1293/(TK+77)]exp(0.00004P)

c. P<1200 MPa, TS1=889+17900/(P+54)+20200/(P+54)^2; P>1200 MPa, TS1=831+0.06P. TL1=1262+0.09P

   P<1600 MPa, TS2=973−70400/(P+354)+778×10^5/(P+354)^2; P>1600 MPa, TS2=935+0.0035P+0.0000062P^2. TL2=1423+0.105P

d. See Table S1.

els

α (K⁻¹)	β (MPa)	Viscosity[d]	Sin(φ_{eff})
0	0	A*	0
0	0	A*	0
3×10^{-5}	1×10^{-5}	B*	0.15
		G*	0.06
3×10^{-5}	1×10^{-5}	B*	0.15
		G*	0.06
3×10^{-5}	1×10^{-5}	C*	0.15
		G*	0.06
3×10^{-5}	1×10^{-5}	D*	0.15
		H*	0.06
3×10^{-5}	1×10^{-5}	E*	0.6
			0.06
3×10^{-5}	1×10^{-5}	F*	0.6
			0.06
3×10^{-5}	1×10^{-5}	D*	0.15
		H*	0.06
3×10^{-5}	1×10^{-5}	D*	0.15
		H*	0.06
3×10^{-5}	1×10^{-5}	D*	0.15
		H*	0.06
3×10^{-5}	1×10^{-5}	E*	0.6
			0.06
3×10^{-5}	1×10^{-5}	E*	0.6
			0.06

dioactive heat; α = coefficient of thermal expansion; β = coefficient of